Journal of
Marine Science and Engineering

MDPI

Article

Adaptive Fixed-Time Control Framework for Deterministic Response of Fully Constrained Vessels with Unknown Dynamics

Qiang Guo [1,*], Shuangpeng Duan [1], Jia Zhou [1], Shengguo Wang [1], Rui Li [1] and Xianku Zhang [2]

[1] Xi'an Key Laboratory of Electrical Equipment Condition Monitoring and Power Supply Security, Xi'an University of Science and Technology, Xi'an 710054, China; 17805445653@163.com (S.D.); jiazhouzzz@163.com (J.Z.); 17835918905@163.com (S.W.); lirui203918@163.com (R.L.)
[2] Laboratory of Marine Simulation and Control, Dalian Maritime University, Dalian 116026, China; zhangxk@dlmu.edu.cn
* Correspondence: qiangguo@xust.edu.cn

Abstract

To achieve precise trajectory tracking for surface vessels subject to unknown dynamics, strict physical limitations, and external disturbances, this paper proposes an Adaptive Fixed-Time Control Framework that ensures a deterministic response under full constraints. First, navigation safety is guaranteed by employing a Barrier Lyapunov Function (BLF) to strictly confine vessel position states, enabling constrained position tracking without requiring prior knowledge of the desired trajectory. Second, addressing the input constraint aspect of the "full constraints" problem, a fixed-time auxiliary system is introduced to compensate for nonlinearities induced by actuator saturation, thereby maintaining control feasibility. Central to this framework is the realization of a deterministic response; by incorporating fixed-time convergence theory, the controller guarantees that velocity tracking errors converge within a predefined time bound independent of initial conditions. Furthermore, an RBF neural network combined with adaptive techniques is utilized to estimate unknown dynamics and external disturbance bounds online, enhancing robustness and safety in realistic marine environments.

Keywords: vessel trajectory tracking; input constraints; global fixed-time convergence; adaptive sliding mode control

1. Introduction

With the continuous increase in maritime traffic density, vessels are exposed to significantly elevated safety risks during navigation. Achieving safe and stable trajectory tracking for vessels operating in complex marine environments has therefore become an important research topic in the field of marine motion control [1,2]. In practical navigation scenarios, vessel systems commonly suffer from issues such as the unavailability of predefined desired trajectories, control input constraints imposed by actuator physical limitations, and the coexistence of external disturbances and model uncertainties. These factors severely restrict the improvement of trajectory tracking performance. Therefore, it is of great engineering significance and practical value to design a vessel trajectory tracking control method with fast convergence characteristics while simultaneously considering state constraints, input saturation, and uncertain disturbances.

Precise and efficient tracking control is a key step in achieving autonomous navigation. Although the technology has been continuously advancing and improving under the research of scholars, vessel trajectory tracking control still faces multiple technical challenges.

Academic Editor: Xinqiang Chen

Received: 20 May 2026
Revised: 18 June 2026
Accepted: 20 June 2026
Published: 23 June 2026

On the one hand, during navigation, vessels need to avoid obstacles and comply with the boundary restrictions of navigation areas, with actual position states subject to physical constraints [3]. Moreover, in some scenarios, the desired trajectory is difficult to obtain precisely in advance, limiting the application of traditional preset performance control methods [4]. On the other hand, the vessel's dynamic system is characterized by strong nonlinearity, parameter uncertainty, and is subject to time-varying external disturbances such as wind, waves, and currents. Additionally, actuators such as propellers and rudders [5] have input saturation characteristics, making it difficult for conventional control methods to balance error convergence speed and control stability [6,7]. Furthermore, the real-time response requirements for vessels in marine tasks are increasing. How to achieve rapid convergence of speed tracking errors under complex constraints has become the key to improving trajectory tracking performance [8,9]. However, the introduction of BLF typically leads to a significant increase in control gain when errors approach the boundary, which may easily drive the control command beyond actuator physical limits, thus inducing input saturation. Most existing BLF-based methods lack simultaneous compensation for saturation, potentially degrading practical control performance.

Motivated by the aforementioned challenges, ensuring navigation safety has become a primary concern, prompting research efforts to concentrate on the effective handling of state constraint problems for vessels operating in complex waterways when the desired trajectory cannot be obtained in advance [10–12]. In this direction, preset performance control, as an innovative method for addressing transient performance issues in nonlinear systems [13], employs a core logic of limiting the tracking error within a preset range by designing performance functions and error transformations [14]. However, this method is limited in scenarios where the desired trajectory cannot be obtained in advance, making it difficult to ensure navigation safety. To address this, refs. [15–17] proposed the use of BLF to ensure that the preset performance boundaries are not exceeded by transforming the error, effectively compensating for this deficiency. Ref. [18] further introduced the general BLF into underactuated vessel control, solving the output constraint problem in narrow waterway navigation for the first time. However, while the introduction of state constraints via BLF enhances safety, it inherently introduces a critical side effect: the control gain tends to increase sharply as the tracking error approaches the constraint boundary. This high-gain characteristic directly amplifies the control command, making it more likely to reach or exceed actuator physical limits, thereby inducing input saturation. Input saturation not only degrades tracking performance but may also violate the conditions required for Lyapunov stability analysis. This coupling effect between BLF and input saturation has been observed in several recent vessel control studies. For instance, ref. [19] noted that BLF-based controllers often demand excessive control efforts near constraints, yet their work primarily focused on fault-tolerant performance rather than saturation analysis. Ref. [20] combined BLF with auxiliary systems to mitigate saturation, but the root cause, BLF-induced gain amplification, was not systematically examined. Ref. [21] employed robust neural adaptive control to handle saturation under state constraints, treating saturation as an external disturbance rather than a consequence of the BLF structure. Therefore, within constrained control frameworks that employ BLF, addressing actuator saturation is not merely an additional requirement but a necessary condition for ensuring closed-loop stability and feasibility. Consequently, how to simultaneously enforce state constraints and prevent input saturation while preserving fixed-time convergence becomes an unresolved challenge that motivates this work. To address this challenge, related solutions have evolved from single constraint compensation to multi-layer cooperative control [22,23]. For fixed-time tracking scenarios, ref. [21] compensated for the amplitude deviation between the control command and the actuator output through auxiliary variables, simplifying the computational complexity. However, it only focused on amplitude constraints and did not address the causes of saturation under multi-source disturbances. For distributed multi-agent cooperative scenarios, ref. [24] designed a fast adaptive compensation law to compensate for the deviation between the actuator output and the command within a predetermined time, ensuring that the command does not exceed the actuator output limit. For scenarios where model uncertainties and external disturbances coexist, ref. [25] introduced a robust neural adaptive scheme to directly handle saturation through fixed-time auxiliary variables, combining RBF neural networks to approximate unmodeled dynamics and using robust damping terms to suppress disturbances. This approach reduces saturation risks from both saturation compensation and disturbance suppression dimensions, significantly enhancing practicality. Ref. [26] optimizes the error convergence characteristics by using the performance function of the predetermined time, constrains the filter to limit the input amplitude, and eliminates the saturation deviation through the adaptive law, achieving high-precision control under complex working conditions.

On the basis of ensuring navigation safety and the realizability of control inputs, fast convergence of trajectory tracking errors has become a core objective for further improving control performance [27,28]. Ref. [29] proposes a one-way global terminal sliding mode algorithm, combined with an adaptive approach law to achieve command tracking and accelerate the convergence process. Although it has a fast response, its application scenarios are relatively limited. Ref. [30] adopts backstepping sliding mode and a new sliding mode control, using a double-power convergence law to accelerate the error convergence in stages. The structure is simple, but the robustness of the design is slightly weak. Ref. [31] designs an adaptive integral terminal sliding mode control, integrating the backstepping idea and dead zone technology, and uses a new saturation function to suppress chattering, achieving rapid convergence even under complex trajectories such as spirals. Ref. [32] proposes a second-order fast adaptive nonsingular integral terminal sliding mode controller, combined with an unscented Kalman filter optimized through singular value decomposition and a charging system search algorithm, to dynamically estimate the disturbance boundary and eliminate chattering, achieving rapid error convergence under complex disturbances. The method integrates multiple technologies and has strong robustness. Moreover, related research has found that the fixed-time control theory further optimizes the convergence characteristics [33,34], with global consistent rapid convergence performance. For instance, ref. [35] achieves fixed-time convergence through high-order filters, but it relies on the boundedness assumption of disturbances, limiting global consistency. Ref. [36] covers the entire state with a double-power sliding surface, uses a Taylor predictor to compensate for initial delays in advance, and achieves global consistent rapid convergence under constraint optimization. Ref. [37] incorporates attitude constraints into the fixed-time sliding surface, uses a potential function to ensure global compliance, and employs an adaptive law to compensate for uncertainties, ensuring that the convergence speed and time are globally consistent while considering constraints and robustness. However, when applying fixed-time control to underactuated vessels, the coupling effect of state constraints and input saturation has largely been overlooked [38,39]. Although some recent works have addressed either fixed-time control with input saturation [40,41] or fixed-time control with state constraints [42,43], the simultaneous consideration of both constraints remains largely unexplored. The interaction between BLF-induced high gain and actuator saturation becomes particularly critical under fixed-time convergence requirements, where aggressive control actions are inherently demanded. To date, a unified framework that rigorously handles this coupling while preserving fixed-time stability guarantees has not been established for underactuated vessel trajectory tracking. Beyond the coupling issue between constraints and saturation, another critical gap lies in the handling of unknown dynamics and external disturbances. Although neural networks have been widely used to approximate model uncertainties [44,45] and disturbance observers have been developed to estimate external disturbances [46,47], these methods are typically designed separately. This separate treatment ignores the fact that model uncertainties and external disturbances coexist and interact in complex marine environments, forming compound disturbances. More importantly, existing studies mostly deal with model uncertainties [48] or external disturbances [49] separately, lacking an adaptive estimation and compensation mechanism for the upper bound of compound disturbances, making it difficult to handle the superposition of multiple disturbances in complex marine environments. Therefore, how to draw on the optimization strategies of sliding mode control from multiple fields to achieve global fixed-time convergence of errors under multiple constraints has become an important research direction in the current field of vessel trajectory tracking control.

In response to the above research deficiencies, this paper proposes a fixed-time vessel trajectory tracking control method considering state constraints. By using a BLF to constrain the actual position of the vessels, the navigation safety problem is solved in scenarios where the expected trajectory is unknown; a fixed-time auxiliary system is designed to handle the input saturation nonlinear term, combined with a fixed-time sliding surface to achieve global fixed-time convergence of the speed tracking error; an RBF neural network is used to approximate the model uncertainty term, and an adaptive technique is employed to estimate the upper bound of compound disturbances, enhancing the system's disturbance resistance. The main contributions of this paper are as follows:

- Departing from asymptotic approaches, an RBF neural network is embedded within a fixed-time architecture to estimate unknown dynamics. This ensures model uncertainties are compensated for within a strict, initial-state-independent time window, thereby providing the fast adaptation necessary for the system's deterministic response.
- A dual-constraint mechanism is developed to ensure strict adherence to full constraints. By employing a symmetric Barrier Lyapunov Function (BLF), the framework establishes a "virtual safety corridor" that strictly confines position errors, guaranteeing navigation safety without prior trajectory knowledge. Concurrently, a fixed-time auxiliary system compensates for actuator saturation, ensuring control inputs remain feasible even when system demands exceed physical limits.
- The proposed controller guarantees a deterministic response for the closed-loop system. Leveraging fixed-time stability theory, tracking errors are proven to converge to a small neighborhood of the origin within a predefined time bound. This settling time depends solely on design parameters and is independent of initial states, offering predictable, time-guaranteed performance for time-critical marine missions.

The subsequent chapters of this paper are arranged as follows: In Section 2, a mathematical model of underactuated vessels considering input saturation and compound disturbances is established; in Section 3, the trajectory tracking controller and adaptive law are designed in detail, and the stability of the system is verified through Lyapunov theory; in Section 4, the stability is analyzed; in Section 5, the effectiveness of the proposed control method is verified through simulation experiments; in Section 6, the paper is summarized.

2. Problem Formulation and Preliminaries

2.1. Problem Formulation

With the increase in maritime traffic volume, the risk of navigation safety also rises. When the expected trajectory cannot be obtained in advance, the application of preset performance control will be subject to certain limitations and cannot ensure safety during navigation. Secondly, the acceleration of the error convergence rate will inevitably be accompanied by an increase in control input. However, due to the characteristics of the actuator, there is a certain limit to the control input. Therefore, how to achieve a faster convergence speed under the condition that the control input has a limit is also a technical challenge. In addition to the above issues that need to be considered, vessels navigating at sea will inevitably face the interference of external wind and waves, and the mathematical model of the vessel cannot be precisely obtained. Therefore, the research of this paper is of great significance. This paper aims to design a fixed-time vessel trajectory tracking control method considering state constraints. Figure 1 shows the control system framework:

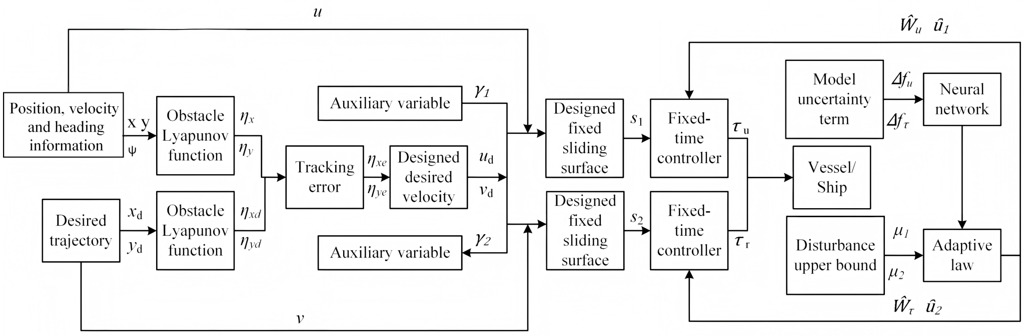

Figure 1. Control system framework.

After considering the input saturation, the mathematical model of the underactuated vessel can be expressed as follows:

$$\begin{cases} \dot{x} = u\cos(\psi) - v\sin(\psi) \\ \dot{y} = u\sin(\psi) + v\cos(\psi) \\ \dot{\psi} = r \\ \dot{u} = \dfrac{(m_{22}v - d_{11}u - \Delta f_u) + \text{sat}(\tau_u) + \tau_{wu}}{m_{11}} \\ \dot{v} = \dfrac{(-m_{11}u - d_{22}v - \Delta f_v) + \tau_{wv}}{m_{22}} \\ \dot{r} = \dfrac{(m_{11} - m_{22})uv - d_{33}r - \Delta f_r + \text{sat}(\tau_r) + \tau_{wr}}{m_{33}} \end{cases} \tag{1}$$

where x, y and ψ denote the surge displacement, sway displacement and yaw angle of the vessel, respectively; u, v and r are the surge velocity, sway velocity and yaw angular velocity in the body-fixed frame. $\text{sat}(\tau_i)$ represents the saturated surge control force and yaw control torque, as defined in Equation (2). m_{11}, m_{22} and m_{33} are the inertial parameters, while d_{11}, d_{22} and d_{33} are the hydrodynamic damping coefficients. Δf_u, Δf_v and Δf_r represent the model uncertainties of the vessel. τ_{wu}, τ_{wv} and τ_{wr} denote the unknown external marine disturbances.

Among

$$\text{sat}(\tau_i) = \begin{cases} \tau_{i_{\max}} & \text{if } \tau_i > \tau_{i_{\max}}, \\ \tau_i & \text{if } \tau_{i_{\min}} \le \tau_i \le \tau_{i_{\max}}, \quad (i = u, r) \\ \tau_{i_{\min}} & \text{if } \tau_i < \tau_{i_{\min}} \end{cases} \tag{2}$$

where $\tau_{i,\max}$ and $\tau_{i,\min}$ represent the upper and lower bounds of the control input, respectively; τ_i is the actual control input.

2.2. Preliminaries

2.2.1. Lemma

Lemma 1. *For any $\varepsilon > 0$, the following inequality holds:*

$$0 \le |s| - s\tanh\left(\frac{s}{\varepsilon}\right) \le 0.2785\varepsilon \tag{3}$$

In the formula, s is an arbitrary variable, and ε is an arbitrary number.

Lemma 2. *For any continuous and smooth function $f(x)$ defined on a compact set $\Omega \subset \mathbb{R}^n$, we have*

$$f(x) = W^{\mathrm{T}}h(x) + o, \quad \forall x \in \Omega \tag{4}$$

where o denotes the approximation error. For all $x \in \Omega$, there exists a vector $o^* > 0$ such that $|o| \le o^*$; W is the weight vector under ideal conditions, which is usually not easily obtainable and treated as an unknown variable, so it needs to be estimated. W^{T} is the transpose of W. $h(x)$ is a Gaussian function, whose expression is given in Equation (5):

$$h(x) = \exp\left(-\frac{\|x - m_j\|^2}{2b_j}\right) \tag{5}$$

where $j = 1, 2, 3, \ldots, n$ is the number of network nodes; m_j is the input center vector; b_j is the standard deviation of the Gaussian function.

Lemma 3. *Consider a dynamic system $\dot{x} = f(x), x(0) = x_0$, where $x \in \mathbb{R}^n$ is the state of the system and x_0 is the equilibrium point of the system. If there exists a Lyapunov function $V(x)$ satisfying Equation (6), then the system is practically fixed-time stable, and the settling time T_r satisfies $T_r \le T_{max} = \frac{1}{\chi\chi_1(j-1)} + \frac{1}{\chi\chi_2(1-q)}$, where $\chi_1 > 0$, $\chi_2 > 0$, $j > 1$, $0 < q < 1$, $\nabla > 0$, $0 < \chi < 1$.*

$$\dot{V}(x) \le -\chi_1 V^j(x) - \chi_2 V^q(x) + \nabla \tag{6}$$

Lemma 4. *If $\xi, \Phi \in \mathbb{R}$, $\delta > 0$, $m > 1$, $n > 1$, and $(m-1)(n-1) = 1$, then the following inequality holds:*

$$\xi\Phi \le \frac{\delta^m}{m}|\xi|^m + \frac{1}{n\delta^n}|\Phi|^n \tag{7}$$

2.2.2. Assumption

Assumption 1. *The external disturbances τ_{wu} and τ_{wr} acting on the vessel are time-varying and bounded with unknown bounds, and possess first-order derivatives.*

Assumption 1 requires that the external disturbances be bounded. In practical marine environments, impulsive disturbances such as sudden wind gusts or wave impacts may temporarily generate large disturbance peaks. Nevertheless, these disturbances remain physically bounded due to the limitations of environmental energy and vessel dynamics. Therefore, Assumption 1 remains valid even under impulsive disturbances.

The proposed adaptive neural approximation mechanism together with the fixed-time robust compensation term can effectively attenuate such disturbance peaks. Although transient control effort may increase during severe disturbances, the auxiliary saturation compensation system prevents excessive actuator commands and ensures that the overall control effort does not become excessive, thereby preserving closed-loop stability.

Assumption 2. *The desired trajectory (x_d, y_d) of the vessel is smooth, and its first-order and second-order derivatives exist.*

3. Controller Design

3.1. Position Constraints Based on Barrier Lyapunov Function

The actual positions x and y of the vessels are constrained using BLF η_x and η_y, and their specific expressions are given in Equation (8):

$$\begin{cases} \eta_x = \ln(x - x_{\min}) - \ln(x_{\max} - x) \\ \eta_y = \ln(y - y_{\min}) - \ln(y_{\max} - y) \end{cases} \tag{8}$$

In the formula, η_x and η_y denote the longitudinal and lateral positions of the vessel after being constrained by the BLF. $x_{\min}$ and $x_{\max}$ are the minimum and maximum allowable longitudinal positions of the vessel, while $y_{\min}$ and $y_{\max}$ are the minimum and maximum allowable lateral positions.

Define η_{xd} and η_{yd} as shown in Equation (9):

$$\begin{cases} \eta_{xd} = \ln(x_d - x_{\min}) - \ln(x_{\max} - x_d) \\ \eta_{yd} = \ln(y_d - y_{\min}) - \ln(y_{\max} - y_d) \end{cases} \tag{9}$$

where η_{xd} and η_{yd} denote the longitudinal and lateral desired positions of the vessel after being constrained by the BLF.

Define the tracking errors η_{xe} and η_{ye} as shown in Equation (10):

$$\begin{cases} \eta_{xe} = \eta_x - \eta_{xd} \\ \eta_{ye} = \eta_y - \eta_{yd} \end{cases} \tag{10}$$

3.2. Design of Desired Velocity

Next, we will design the longitudinal desired velocity u_d and lateral desired velocity v_d that can drive the tracking errors η_{xe} and η_{ye} to converge. If η_{xe} and η_{ye} converge, then η_{xe} and η_{ye} must be bounded, and thus the constraints on the actual positions x and y of the vessel can be satisfied, as shown in Equation (11):

$$\begin{cases} x_{\min} < x < x_{\max} \\ y_{\min} < y < y_{\max} \end{cases} \tag{11}$$

Taking the derivative of Equation (10) yields the following:

$$\begin{cases} \dot{\eta}_{xe} = \dfrac{(x_{\max} - x_{\min})\dot{x} - \dot{x}_{\min}(x_{\max} - x) - \dot{x}_{\max}(x - x_{\min})}{(x - x_{\min})(x_{\max} - x)} - \dot{\eta}_{xd} \\ \dot{\eta}_{ye} = \dfrac{(y_{\max} - y_{\min})\dot{y} - \dot{y}_{\min}(y_{\max} - y) - \dot{y}_{\max}(y - y_{\min})}{(y - y_{\min})(y_{\max} - y)} - \dot{\eta}_{yd} \end{cases} \tag{12}$$

where the expressions of $\dot{\eta}_{xd}$ and $\dot{\eta}_{yd}$ are given in Equation (13):

$$\begin{cases} \dot{\eta}_{xd} = \dfrac{(x_{\max} - x_{\min})\dot{x}_d - \dot{x}_{\min}(x_{\max} - x_d) - \dot{x}_{\max}(x_d - x_{\min})}{(x_d - x_{\min})(x_{\max} - x_d)} \\ \dot{\eta}_{yd} = \dfrac{(y_{\max} - y_{\min})\dot{y}_d - \dot{y}_{\min}(y_{\max} - y_d) - \dot{y}_{\max}(y_d - y_{\min})}{(y_d - y_{\min})(y_{\max} - y_d)} \end{cases} \tag{13}$$

https://doi.org/10.3390/jmse14131150

Based on Equation (12), to drive η_{xe} and η_{ye} to converge, $\dot{x}$ and $\dot{y}$ can be designed as follows:

$$\begin{cases} \dot{x} = \dfrac{\dot{x}_{\min}(x_{\max} - x) + \dot{x}_{\max}(x - x_{\min})}{x_{\max} - x_{\min}} + \dfrac{(x - x_{\min})(x_{\max} - x)}{x_{\max} - x_{\min}}\dot{\eta}_{xd} \\ \quad - k_1 \dfrac{\eta_{xe}(x - x_{\min})(x_{\max} - x)}{x_{\max} - x_{\min}}, \\ \dot{y} = \dfrac{\dot{y}_{\min}(y_{\max} - y) + \dot{y}_{\max}(y - y_{\min})}{y_{\max} - y_{\min}} + \dfrac{(y - y_{\min})(y_{\max} - y)}{y_{\max} - y_{\min}}\dot{\eta}_{yd} \\ \quad - k_2 \dfrac{\eta_{ye}(y - y_{\min})(y_{\max} - y)}{y_{\max} - y_{\min}}. \end{cases} \tag{14}$$

where k_1 and k_2 are positive parameters to be designed. Combining Equations (1) and (14), we obtain the following:

$$\begin{cases} \dot{x} = \dfrac{\dot{x}_{\min}(x_{\max} - x) + \dot{x}_{\max}(x - x_{\min})}{x_{\max} - x_{\min}} + \dfrac{(x - x_{\min})(x_{\max} - x)}{x_{\max} - x_{\min}}\dot{\eta}_{xd} \\ \quad - k_1 \dfrac{\eta_{xe}(x - x_{\min})(x_{\max} - x)}{x_{\max} - x_{\min}} \\ \quad = u\cos\psi - v\sin\psi, \\ \dot{y} = \dfrac{\dot{y}_{\min}(y_{\max} - y) + \dot{y}_{\max}(y - y_{\min})}{y_{\max} - y_{\min}} + \dfrac{(y - y_{\min})(y_{\max} - y)}{y_{\max} - y_{\min}}\dot{\eta}_{yd} \\ \quad - k_2 \dfrac{\eta_{ye}(y - y_{\min})(y_{\max} - y)}{y_{\max} - y_{\min}} \\ \quad = u\sin\psi + v\cos\psi. \end{cases} \tag{15}$$

For convenience of description, define z_x and z_y as shown in Equation (16):

$$\begin{cases} z_x = \dfrac{\dot{x}_{\min}(x_{\max} - x) + \dot{x}_{\max}(x - x_{\min})}{x_{\max} - x_{\min}} + \dfrac{(x - x_{\min})(x_{\max} - x)}{x_{\max} - x_{\min}}\dot{\eta}_{xd} \\ \quad - k_1 \dfrac{\eta_{xe}(x - x_{\min})(x_{\max} - x)}{x_{\max} - x_{\min}}, \\ z_y = \dfrac{\dot{y}_{\min}(y_{\max} - y) + \dot{y}_{\max}(y - y_{\min})}{y_{\max} - y_{\min}} + \dfrac{(y - y_{\min})(y_{\max} - y)}{y_{\max} - y_{\min}}\dot{\eta}_{yd} \\ \quad - k_2 \dfrac{\eta_{ye}(y - y_{\min})(y_{\max} - y)}{y_{\max} - y_{\min}}. \end{cases} \tag{16}$$

Based on Equation (15), the desired longitudinal velocity u_d and desired lateral velocity v_d can be designed as follows:

$$\begin{cases} u_d = z_x\cos(\psi) + z_y\sin(\psi) \\ v_d = z_x(-\sin(\psi)) + z_y\cos(\psi) \end{cases} \tag{17}$$

When u approaches u_d and v approaches v_d, Equation (12) can be simplified to the following:

$$\begin{cases} \dot{\eta}_{xe} = -k_1\eta_{xe} \\ \dot{\eta}_{ye} = -k_2\eta_{ye} \end{cases} \tag{18}$$

Define the Lyapunov function V_1 as shown in Equation (19):

$$V_1 = \frac{1}{2}\eta_{xe}^2 + \frac{1}{2}\eta_{ye}^2 \tag{19}$$

Taking the derivative of Equation (19) and substituting Equation (18) into it, we get the following:

$$\begin{aligned} \dot{V}_1 &= \eta_{xe}\dot{\eta}_{xe} + \eta_{ye}\dot{\eta}_{ye} \\ &= -k_1\eta_{xe}^2 - k_2\eta_{ye}^2 \\ &\leq -\varsigma_1 V_1 \end{aligned} \tag{20}$$

where

$$\varsigma_1 = \min(2k_1, 2k_2) \tag{21}$$

From Equation (20), when u converges to u_d and v converges to v_d, η_{xe} and η_{ye} can converge, which in turn enables the constraints on the actual positions x and y of the vessel to be satisfied.

Next, considering the input saturation, we will design the longitudinal control force τ_u and yaw control torque τ_r to drive the actual velocity of the vessel to approach the desired velocity.

Taking the derivative of Equation (17) and simplifying it, we obtain the following:

$$\begin{cases} \dot{u}_d = rv_d + \dot{z}_x\cos(\psi) + \dot{z}_y\sin(\psi) \\ \dot{v}_d = -ru_d + \dot{z}_x(-\sin(\psi)) + \dot{z}_y\cos(\psi) \end{cases} \tag{22}$$

where $\dot{z}_x$ and $\dot{z}_y$ are the first-order derivatives of z_x and z_y, respectively.

3.3. Sliding Mode Control Design

To avoid unconstrained input τ_u during the controller design process, a fixed-time auxiliary variable γ_1 is introduced into the velocity tracking error u_e. The specific expression of u_e is given in Equation (23):

$$u_e = u - u_d - \gamma_1 \tag{23}$$

The fixed-time sliding surface s_1 is defined as in (24).

$$\begin{aligned} s_1 = u_e + \lambda_1\int_0^t u_e\,\mathrm{d}t + \lambda_2\int_0^t \tanh(u_e)\,\mathrm{d}t \\ + \lambda_3\int_0^t u_e^{\theta-1}\tanh(u_e^{\theta})\,\mathrm{d}t. \end{aligned} \tag{24}$$

where λ_1, λ_2 and λ_3 are positive parameters to be designed, and $\theta > 1$.

Taking the derivative of Equation (24) and combining it with Equations (1) and (23), we obtain the following:

$$\begin{aligned} \dot{s}_1 = \frac{m_{22}vr - d_{11}u - \Delta f_u + \mathrm{sat}(\tau_u) + \tau_{wu}}{m_{11}} - \dot{u}_d - \dot{\gamma}_1 \\ + \lambda_1(u - u_d - \gamma_1) + \lambda_2\tanh(u_e) + \lambda_3 u_e^{\theta-1}\tanh(u_e^{\theta}) \end{aligned} \tag{25}$$

Let

$$\dot{\gamma}_1 = -\lambda_1\gamma_1 - k_1\tanh(\gamma_1) + \frac{\mathrm{sat}(\tau_u) - \tau_u}{m_{11}} \tag{26}$$

By transforming Equation (25) using the fixed-time auxiliary variable γ_1, Equation (25) can be rewritten as Equation (27):

$$\begin{aligned}\dot{s}_1 = &\frac{m_{22}vr - d_{11}u - \Delta f_u + \tau_u + \tau_{wu}}{m_{11}} \\ &- \dot{u}_d + \lambda_1(u - u_d) + \lambda_2 \tanh(u_e) + \lambda_3 u_e^{\theta-1} \tanh(u_e^{\theta})\end{aligned} \tag{27}$$

3.4. RBF-Based Adaptive Law Design

Since RBF neural networks have the universal approximation capability for any smooth function, we use the neural network to estimate Δf_u. According to Lemma 2, the neural network output expression of the unknown term Δf_u is given in Equation (28):

$$\Delta f_u = \boldsymbol{W}_u^T h_u(x) + o_1 \tag{28}$$

where $\boldsymbol{W}_u$ is the weight matrix of Δf_u, $h_u(x)$ is the Gaussian function used to estimate Δf_u, and o_1 is the estimation error of Δf_u.

Combining Equation (28), the control input τ_u can be designed as shown in Equation (29):

$$\begin{aligned}\tau_u = &-m_{22}vr + d_{11}u + \hat{\boldsymbol{W}}_u^T h_u(x) - \hat{\mu}_1 \tanh(s_1/\varepsilon_1) + m_{11}\dot{u}_d \\ &- m_{11}\lambda_1(u - u_d) - m_{11}\left(\lambda_2 \tanh(u_e) + \lambda_3 u_e^{\theta-1} \tanh(u_e^{\theta})\right) \\ &- m_{11}k_1 \tanh(\gamma_1) - c_3 s_1^3 - c_4 \mathrm{sign}(s_1)\end{aligned} \tag{29}$$

where c_3, c_4 and ε_1 are positive design parameters. $\phi_1 = -o_1 + \tau_{wu}$, μ_1 is the upper bound of ϕ_1, and $\hat{\mu}_1$ is the estimate of μ_1. The adaptive laws for parameters $\hat{\boldsymbol{W}}_u$ and $\hat{\mu}_1$ are given in Equation (30):

$$\begin{cases}\dot{\hat{\boldsymbol{W}}}_u = \eta_1\left(-s_1 h_u(x) - \sigma_1 \hat{\boldsymbol{W}}_u^3 - \sigma_2 \hat{\boldsymbol{W}}_u\right) \\ \dot{\hat{\mu}}_1 = \eta_2\left(s_1 \tanh(s_1/\varepsilon_1) - \sigma_3 \hat{\mu}_1^3 - \sigma_4 \hat{\mu}_1\right)\end{cases} \tag{30}$$

where η_1, η_2, σ_1, σ_2, σ_3 and σ_4 are positive design parameters.

Let

$$v_e = v - v_d - \int_0^t \gamma_2 \mathrm{d}t \tag{31}$$

Define the sliding surface s_2 as shown in Equation (32):

$$s_2 = v_e + \lambda_4 v_e + \lambda_5 \tanh(v_e) + \lambda_6 v_e^{\delta-1} \tanh(v_e^{\delta}) \tag{32}$$

where λ_4, λ_5 and λ_6 are positive design parameters.

For the convenience of subsequent notation, let

$$f = \dot{z}_x(-\sin(\psi)) + \dot{z}_y \cos(\psi) \tag{33}$$

Then $v_d = -ru_d + f$, and its derivative is given in Equation (34):

$$\dot{v}_d = -\dot{r}u_d - r\dot{u}_d + \dot{f} \tag{34}$$

To avoid the "differential explosion" problem caused by directly differentiating f, a dynamic surface will be designed to replace the differentiation process of f, and its expression is as follows:

$$T_r \dot{f}_r + f_r = f,\ f_r(0) = f(0) \tag{35}$$

where $T_r > 0$ is a design parameter.

Taking the derivative of Equation (32) and combining it with Equations (1), (31) and (34), we obtain the following:

$$\begin{aligned}\dot{s}_2 &= \dot{v}_e + \lambda_4 \dot{v}_e + \lambda_5\left(1 - \tanh^2(v_e)\right)\dot{v}_e \\ &\quad + \lambda_6\left((\theta-1)v_e^{\theta-2}\tanh(v_e^{\theta}) + v_e^{\theta-1}\left(1-\tanh^2(v_e^{\theta})\right)\theta v_e^{\theta-1}\right)\dot{v}_e \\ &= \frac{m_{22}u_d - m_{11}u}{m_{22}}\left(\frac{(m_{11}-m_{22})vr - d_{33}r - \Delta f_r + \mathrm{sat}(\tau_r) + \tau_{wr}}{m_{33}}\right) \\ &\quad - \dot{\gamma}_2 - \lambda_4\gamma_2 + \Delta\end{aligned} \tag{36}$$

where

$$\begin{aligned}\Delta &= \frac{-m_{11}\dot{u} - d_{22}\dot{v} - \Delta\dot{f}_v + \tau_{wv}}{m_{22}} + r\dot{u}_d - \dot{f}_r \\ &\quad + \lambda_4(\dot{v} - \dot{v}_d) + \lambda_5\left(1 - \tanh^2(v_e)\right)(\dot{v} - \dot{v}_d) \\ &\quad + \lambda_6\left((\theta-1)v_e^{\theta-2}\tanh(v_e^{\theta}) + v_e^{\theta-1}\left(1-\tanh^2(v_e^{\theta})\right)\theta v_e^{\theta-1}\right)\dot{v}_e\end{aligned} \tag{37}$$

The fixed-time auxiliary variable γ_2 is used to transform Equation (36), so that the unconstrained yaw control torque τ_r can be introduced.

Let

$$\begin{aligned}\dot{\gamma}_2 &= -\lambda_4\gamma_2 - \lambda_5\left(1 - \tanh^2(v_e)\right)\gamma_2 - k_2\tanh(\gamma_2) \\ &\quad + \left(\frac{m_{22}u_d - m_{11}u}{m_{22}}\right)\frac{\mathrm{sat}(\tau_r) - \tau_r}{m_{33}}\end{aligned} \tag{38}$$

The RBF neural network is used to estimate the unknown term Δf_r, and its specific expression is as follows:

$$\Delta f_r = \boldsymbol{W}_r^T h_r(x) + \sigma_2 \tag{39}$$

where $\boldsymbol{W}_r$ is the weight matrix of Δf_r, $h_r(x)$ is the Gaussian function used to estimate Δf_r, and σ_2 is the estimation error of Δf_r.

Based on the fixed-time convergence theory and Equation (36), the control input τ_r can be designed as shown in Equation (40):

$$\begin{aligned}\tau_r &= (m_{22} - m_{11})uv + d_{33}r + \hat{\boldsymbol{W}}_r^T h_r(x) - \hat{\mu}_2\tanh(s_2/\varepsilon_2) \\ &\quad - \frac{m_{33}k_2\tanh(\gamma_2)}{\left(u_d - \frac{m_{11}u}{m_{22}}\right)} - \frac{m_{33}\Delta}{\left(u_d - \frac{m_{11}u}{m_{22}}\right)} - c_5 s_2^3 - c_6\mathrm{sign}(s_2)\end{aligned} \tag{40}$$

where c_5, c_6 and ε_2 are positive design parameters. $\phi_2 = -\sigma_2 + \tau_{wr}$, μ_2 is the upper bound of ϕ_2, and $\hat{\mu}_2$ is the estimate of μ_2. The adaptive laws for parameters $\hat{\boldsymbol{W}}_r$ and $\hat{\mu}_2$ are given in Equation (41):

$$\begin{cases}\dot{\hat{\boldsymbol{W}}}_r = \eta_3\left(-\left(u_d - \frac{m_{11}u}{m_{22}}\right)s_2 h_r(x) - \sigma_5\hat{\boldsymbol{W}}_r^3 - \sigma_6\hat{\boldsymbol{W}}_r\right) \\ \dot{\hat{\mu}}_2 = \eta_4\left(\left(u_d - \frac{m_{11}u}{m_{22}}\right)s_2\tanh(s_2/\varepsilon_2) - \sigma_7\hat{\mu}_2^3 - \sigma_8\hat{\mu}_2\right)\end{cases} \tag{41}$$

where η_3, η_4, σ_5, σ_6, σ_7 and σ_8 are positive design parameters.

4. Stability Analysis

Theorem 1 (Main Result)**.** *Consider the fully constrained underactuated vessel system described by Equation (1), subject to unknown dynamics, external disturbances (Assumption 1), and input saturation. Suppose the desired trajectory satisfies Assumption 2. By applying the designed virtual* *control laws (17), the fixed-time sliding surfaces (24) and (32), the adaptive updating laws (30) and (41), and the final actual control inputs (29) and (40), the following properties are guaranteed for the closed-loop system:*

1. *Practical Fixed-Time Stability: All signals in the closed-loop system are practically fixed-time stable. The velocity tracking errors converge to a small neighborhood of the origin within a predefined settling time T_{max}.*
2. *Deterministic Response: The upper bound of the settling time T_{max} is independent of the initial states of the vessel and can be pre-assigned by tuning the control parameters.*
3. *Full Constraint Satisfaction: The actual positions of the vessel strictly remain within the predefined safe boundaries (i.e., $x_{min} < x < x_{max}$ and $y_{min} < y < y_{max}$) for all $t > 0$, and the control inputs never exceed the actuator physical limits.*

Proof of Theorem 1. We construct a comprehensive Lyapunov candidate function V_2 that incorporates the sliding surfaces and the parameter estimation errors:

$$\begin{aligned} V_2 = \frac{1}{2}m_{11}s_1^2 + \frac{1}{2}m_{33}s_2^2 + \frac{1}{2\eta_1}\tilde{\boldsymbol{W}}_u^T\tilde{\boldsymbol{W}}_u \\ + \frac{1}{2\eta_2}\tilde{\mu}_1^2 + \frac{1}{2\eta_3}\tilde{\boldsymbol{W}}_r^T\tilde{\boldsymbol{W}}_r + \frac{1}{2\eta_4}\tilde{\mu}_2^2 \end{aligned} \tag{42}$$

where $\tilde{\boldsymbol{W}}_u = \hat{\boldsymbol{W}}_u - \boldsymbol{W}_u$, $\tilde{\boldsymbol{W}}_r = \hat{\boldsymbol{W}}_r - \boldsymbol{W}_r$, $\tilde{\mu}_1 = \hat{\mu}_1 - \mu_1$, $\tilde{\mu}_2 = \hat{\mu}_2 - \mu_2$.

Taking the derivative of both sides of Equation (42), we obtain the following:

$$\dot{V}_2 = m_{11}s_1\dot{s}_1 + m_{33}s_2\dot{s}_2 + \frac{1}{\eta_1}\tilde{\boldsymbol{W}}_u^T\dot{\hat{\boldsymbol{W}}}_u + \frac{1}{\eta_2}\tilde{\mu}_1\dot{\hat{\mu}}_1 + \frac{1}{\eta_3}\tilde{\boldsymbol{W}}_r^T\dot{\hat{\boldsymbol{W}}}_r + \frac{1}{\eta_4}\tilde{\mu}_2\dot{\hat{\mu}}_2 \tag{43}$$

For the first term $m_{11}s_1\dot{s}_1$ in Equation (43), combining Equations (27) and (29), we get the following:

$$\begin{aligned} m_{11}s_1\dot{s}_1 &= m_{11}s_1\bigg(\frac{m_{22}vr - d_{11}u - \Delta f_u + \tau_u + \tau_{wu}}{m_{11}} - \dot{u}_d + \lambda_1(u - u_d) + \lambda_2\tanh(u_e) \\ &\quad + \lambda_3 u_e^{\theta-1}\tanh(u_e^{\theta})\bigg) \\ &= s_1\Big(-\boldsymbol{W}_u^T h_u(x) + \hat{\boldsymbol{W}}_u^T h_u(x) + \mu_1 - \hat{\mu}_1\tanh(s_1/\varepsilon_1) - c_3 s_1^3 - c_4\mathrm{sign}(s_1)\Big) \\ &= -c_3 s_1^4 - c_4|s_1| + s_1\Big(\tilde{\boldsymbol{W}}_u^T h_u(x) + \mu_1 - \hat{\mu}_1\tanh(s_1/\varepsilon_1)\Big) \end{aligned} \tag{44}$$

For the second term $m_{33}s_2\dot{s}_2$ in Equation (43), combining Equations (36) to (40), it can be transformed into the following form:

$$\begin{aligned} m_{33}s_2\dot{s}_2 &= m_{33}s_2 \cdot \frac{m_{22}u_d - m_{11}u}{m_{22}} \cdot \frac{(m_{11} - m_{22})uv - d_{33}r - \Delta f_r + \tau_r + \tau_{wr}}{m_{33}} \\ &= s_2 \cdot \frac{m_{22}u_d - m_{11}u}{m_{22}} \cdot \left(-\boldsymbol{W}_r^T h_r(x) + \hat{\boldsymbol{W}}_r^T h_r(x) + \mu_2 - \hat{\mu}_2\tanh\left(\frac{s_2}{\varepsilon_2}\right)\right. \\ &\quad \left. - c_5 s_2^3 - c_6\,\mathrm{sign}(s_2)\right) \\ &= -c_5 \cdot \frac{m_{22}u_d - m_{11}u}{m_{22}} \cdot s_2^4 - c_6 \cdot \frac{m_{22}u_d - m_{11}u}{m_{22}} \cdot |s_2| \\ &\quad + s_2 \cdot \frac{m_{22}u_d - m_{11}u}{m_{22}} \cdot \left(\tilde{\boldsymbol{W}}_r^T h_r(x) + \mu_2 - \hat{\mu}_2\tanh\left(\frac{s_2}{\varepsilon_2}\right)\right) \end{aligned} \tag{45}$$

Combining Equations (44) and (45), Equation (43) can be transformed into the form shown in Equation (46):

$$\begin{aligned}\dot{V}_2 = &-c_3 s_1^4 - c_4|s_1| - c_5 \cdot \frac{m_{22}u_d - m_{11}u}{m_{22}} s_2^4 - c_6 \cdot \frac{m_{22}u_d - m_{11}u}{m_{22}}|s_2| \\ &+ s_1\left(\mu_1 - \hat{\mu}_1 \tanh\left(\frac{s_1}{\varepsilon_1}\right)\right) - \sigma_1 \tilde{\boldsymbol{W}}_u^T \tilde{\boldsymbol{W}}_u - \sigma_2 \tilde{\boldsymbol{W}}_u^T \tilde{\boldsymbol{W}}_u \\ &- \sigma_3 \tilde{\mu}_1 \hat{\mu}_1^3 - \sigma_4 \tilde{\mu}_1 \hat{\mu}_1 + s_2 \cdot \frac{m_{22}u_d - m_{11}u}{m_{22}}\left(\mu_2 - \hat{\mu}_2 \tanh\left(\frac{s_2}{\varepsilon_2}\right)\right) \\ &- \sigma_5 \tilde{\boldsymbol{W}}_r^T \tilde{\boldsymbol{W}}_r - \sigma_6 \tilde{\boldsymbol{W}}_r^T \tilde{\boldsymbol{W}}_r - \sigma_7 \tilde{\mu}_2 \hat{\mu}_2^3 - \sigma_8 \tilde{\mu}_2 \hat{\mu}_2\end{aligned} \tag{46}$$

According to Lemma 4, the term $-\sigma_3 \tilde{\mu}_1 \hat{\mu}_1^3$ in Equation (46) can be transformed into the following:

$$\begin{aligned}-\sigma_3 \tilde{\mu}_1 \hat{\mu}_1^3 &= -\sigma_3 \tilde{\mu}_1 (\tilde{\mu}_1 + \mu_1)^3 \\ &\leq -\sigma_3 \hat{\mu}_1^4 - 3\sigma_3 \hat{\mu}_1^3 \mu_1 - \sigma_3 \tilde{\mu}_1 \hat{\mu}_1^3 \\ &\leq -\sigma_3\left(1 - \frac{9}{4}k_{s1}^{\frac{4}{3}} - \frac{1}{4k_{s2}^{\frac{4}{3}}}\right)\hat{\mu}_1^4 + \sigma_3\left(\frac{3}{4k_{s1}^{\frac{4}{3}}} + \frac{3}{4}k_{s2}^{\frac{4}{3}}\right)|\mu_1|^4\end{aligned} \tag{47}$$

Consider the following inequality:

$$0 \leq \left(\frac{1}{2}|x| - \frac{1}{4}\right)^2 = \frac{1}{4}x^2 - \frac{1}{4}|x| + \frac{1}{16} \implies -\frac{1}{4}x^2 \leq -\frac{1}{4}|x| + \frac{1}{16} \tag{48}$$

Combining Young's inequality and Equation (47), the term $-\sigma_2 \tilde{\boldsymbol{W}}_u^T \tilde{\boldsymbol{W}}_u$ in Equation (46) can be transformed into the following:

$$\begin{aligned}-\sigma_2 \tilde{\boldsymbol{W}}_u^T \tilde{\boldsymbol{W}}_u &= -\sigma_2 \tilde{\boldsymbol{W}}_u^T (\tilde{\boldsymbol{W}}_u + \boldsymbol{W}_u) \\ &\leq \frac{-\sigma_2 \tilde{\boldsymbol{W}}_u^T \tilde{\boldsymbol{W}}_u + \sigma_2 \boldsymbol{W}_u^T \boldsymbol{W}_u}{2} \\ &\leq \frac{-\sigma_2 \tilde{\boldsymbol{W}}_u^T \tilde{\boldsymbol{W}}_u}{4} - \frac{\sigma_2}{4}\|\tilde{\boldsymbol{W}}_u\|^2 + \frac{\sigma_2}{16} + \frac{\sigma_2}{2}\boldsymbol{W}_u^T \boldsymbol{W}_u\end{aligned} \tag{49}$$

Combining Equations (47) and (49), Lemmas 1 and 4, Equation (46) can be transformed into the following:

$$\begin{aligned}\dot{V}_2 \leq &-c_3 s_1^4 - c_4|s_1| - c_5\left(\frac{m_{22}u_d - m_{11}u}{m_{22}}\right)^4 s_2^4 - c_6\left(\frac{m_{22}u_d - m_{11}u}{m_{22}}\right)|s_2| \\ &- \sigma_1\left(1 - \frac{9}{4}k_{u1}^{\frac{4}{3}} - \frac{1}{4k_{u2}^4}\right)\|\tilde{W}_u\|^4 + \sigma_1\left(\frac{3}{4k_{u1}^4} + \frac{3}{4}k_{u2}^{\frac{4}{3}}\right)\|W_u\|^4 \\ &- \frac{\sigma_2}{4}\|\tilde{W}_u\|^2 - \frac{\sigma_2}{4}\|\tilde{W}_u\|^2 + \frac{\sigma_2}{16} + \frac{\sigma_2}{2}W_u^T W_u \\ &- \sigma_3\left(1 - \frac{9}{4}k_{31}^{\frac{4}{3}} - \frac{1}{4k_{32}^4}\right)\tilde{\mu}_1^4 + \sigma_3\left(\frac{3}{4k_{31}^4} + \frac{3}{4}k_{32}^{\frac{4}{3}}\right)\mu_1^4 \\ &- \frac{\sigma_4}{4}\tilde{\mu}_1^2 - \frac{\sigma_4}{4}\tilde{\mu}_1^2 + \frac{\sigma_4}{16} + \frac{\sigma_4}{2}\mu_1^2 \\ \leq &-c_3 s_1^4 - c_5\left(\frac{m_{22}u_d - m_{11}u}{m_{22}}\right)^4 s_2^4 - \sigma_1\left(1 - \frac{9}{4}k_{u1}^{\frac{4}{3}} - \frac{1}{4k_{u2}^4}\right)\|\tilde{W}_u\|^4 \\ &- \sigma_3\left(1 - \frac{9}{4}k_{31}^{\frac{4}{3}} - \frac{1}{4k_{32}^4}\right)\tilde{\mu}_1^4 - \sigma_5\left(1 - \frac{9}{4}k_{51}^{\frac{4}{3}} - \frac{1}{4k_{52}^4}\right)\|\tilde{W}_r\|^4\end{aligned}$$

$$
\begin{aligned}
& -\sigma_7\left(1-\frac{9}{4}k_{71}^{\frac{4}{3}}-\frac{1}{4k_{72}^4}\right)\tilde{\mu}_2^4-c_4|s_1|-c_6\left(\frac{m_{22}u_d-m_{11}u}{m_{22}}\right)|s_2| \\
& -\frac{\sigma_2}{4}\|\tilde{W}_u\|^2-\frac{\sigma_4}{4}\tilde{\mu}_1^2-\frac{\sigma_6}{4}\|\tilde{W}_r\|^2-\frac{\sigma_8}{4}\tilde{\mu}_2^2 \\
& +\sigma_1\left(\frac{3}{4k_{u1}^4}+\frac{3}{4}k_{u2}^{\frac{4}{3}}\right)\|W_u\|^4+\sigma_3\left(\frac{3}{4k_{31}^4}+\frac{3}{4}k_{32}^{\frac{4}{3}}\right)\mu_1^4 \\
& +\sigma_5\left(\frac{3}{4k_{51}^4}+\frac{3}{4}k_{52}^{\frac{4}{3}}\right)\|W_r\|^4+\sigma_7\left(\frac{3}{4k_{71}^4}+\frac{3}{4}k_{72}^{\frac{4}{3}}\right)\mu_2^4 \\
& +\frac{\sigma_2}{2}W_u^TW_u+\frac{\sigma_4}{2}\mu_1^2+\frac{\sigma_6}{2}W_r^TW_r+\frac{\sigma_8}{2}\mu_2^2+\frac{\sigma_2+\sigma_4+\sigma_6+\sigma_8}{16} \\
\leq\ & -\frac{\chi_1}{6}V_2^2-\chi_2V_2^{\frac{1}{2}}+\beta_1.
\end{aligned} \tag{50}
$$

where

$$
\begin{aligned}
\chi_1=\min\Bigg(&\frac{4c_3}{m_{11}^2},\ \frac{4c_5}{m_{33}^2}\left(\frac{m_{22}u_d-m_{11}u}{m_{22}}\right), \\
&4\eta_1^2\sigma_1\left(1-\frac{9}{4}k_{11}^{\frac{4}{3}}-\frac{1}{4k_{12}^4}\right)+4\eta_2^2\sigma_3\left(1-\frac{9}{4}k_{31}^{\frac{4}{3}}-\frac{1}{4k_{32}^4}\right), \\
&4\eta_3^2\sigma_5\left(1-\frac{9}{4}k_{51}^{\frac{4}{3}}-\frac{1}{4k_{52}^4}\right)+4\eta_4^2\sigma_7\left(1-\frac{9}{4}k_{71}^{\frac{4}{3}}-\frac{1}{4k_{72}^4}\right)\Bigg)
\end{aligned} \tag{51}
$$

$$
\begin{aligned}
\chi_2=\min\Bigg(&c_4\sqrt{\tfrac{2}{m_{11}}},\ c_6\left(\tfrac{m_{22}u_d-m_{11}u}{m_{22}}\right)\sqrt{\tfrac{2}{m_{33}}},\ \tfrac{\sigma_2}{4}\sqrt{2\eta_1}, \\
&\tfrac{\sigma_4}{4}\sqrt{2\eta_2},\ \tfrac{\sigma_6}{4}\sqrt{2\eta_3},\ \tfrac{\sigma_8}{4}\sqrt{2\eta_4}\Bigg)
\end{aligned} \tag{52}
$$

$$
\begin{aligned}
\beta_1=\ &\sigma_1\left(\frac{3}{4k_{11}^4}+\frac{3}{4}k_{12}^{\frac{4}{3}}\right)\|\boldsymbol{W}_u\|^4+\sigma_3\left(\frac{3}{4k_{31}^4}+\frac{3}{4}k_{32}^{\frac{4}{3}}\right)|\mu_1|^4 \\
&+\sigma_5\left(\frac{3}{4k_{51}^4}+\frac{3}{4}k_{52}^{\frac{4}{3}}\right)\|\boldsymbol{W}_r\|^4+\sigma_7\left(\frac{3}{4k_{71}^4}+\frac{3}{4}k_{72}^{\frac{4}{3}}\right)|\mu_2|^4 \\
&+\frac{\sigma_2}{2}\boldsymbol{W}_u^T\boldsymbol{W}_u+\frac{\sigma_4}{2}\mu_1^2+\frac{\sigma_6}{2}\boldsymbol{W}_r^T\boldsymbol{W}_r+\frac{\sigma_8}{2}\mu_2^2 \\
&+\frac{\sigma_2+\sigma_4+\sigma_6+\sigma_8}{16}.
\end{aligned} \tag{53}
$$

Based on the derived inequality $\dot{V}\leq-\chi_1V^2-\chi_2V^{\frac{1}{2}}+\beta_1$, and invoking Lemma 3, we can conclude that the closed-loop system is practically fixed-time stable. The settling time T_f is strictly bounded by $T_f\leq T_{max}=\frac{1}{\chi_1(2-1)}+\frac{1}{\chi_2(1-0.5)}=\frac{1}{\chi_1}+\frac{2}{\chi_2}$. This proves that the convergence time T_{max} is entirely determined by the design parameters (χ_1,χ_2) and is completely independent of the initial conditions, thereby guaranteeing a deterministic response.

Furthermore, because the velocity tracking errors s_1 and s_2 converge within T_{max}, the actual velocities u and v track the virtual control laws u_d and v_d. According to the Barrier Lyapunov Function (BLF) analysis in Equation (20), the convergence of velocities ensures that the position tracking errors η_{xc} and η_{yc} remain bounded. Consequently, the actual vessel positions x and y never violate the predefined safety constraints $x_{min}<x<x_{max}$ and $y_{min}<y<y_{max}$. The input saturation is effectively compensated by the fixed-time auxiliary variables γ_1 and γ_2. This completes the proof. □

5. Simulation Experiments

To verify the effectiveness of the control scheme designed in this paper, a computer simulation experiment is conducted using a patrol vessel named BAY CLASS (owned by

Singapore Customs) as the simulation object. The vessel is 38 m long. The hydrodynamic coefficients, model uncertainty terms, and external disturbances are defined as follows.

The external time-varying disturbance is given by the following:

$$\begin{cases} \tau_{wu} = 10^4[\sin(0.2t) + \cos(0.5t)] \\ \tau_{wv} = 10^2[\sin(0.1t) + \cos(0.4t)] \\ \tau_{wr} = 10^5[\sin(0.5t) + \cos(0.3t)] \end{cases} \tag{54}$$

All key control and simulation parameters are systematically listed in Table 1, grouped by their respective functional modules. The parameters are tuned sequentially to ensure stable and satisfactory system performance. Most of the remaining parameters have little influence on system performance. For the dominant control parameters, they can be determined by tuning their values while observing the simulation response. An excessively large or small parameter value will lead to unsatisfactory performance, such as overshoot, slow response, or divergence. Therefore, it is not difficult to narrow down the reasonable range of candidate values and obtain the optimal control parameters. The parameters can be divided into four categories: BLF parameters, fixed-time convergence parameters, adaptive and RBF parameters, and auxiliary system parameters. In practice, the parameters are tuned sequentially: first the constraint boundaries, then the fixed-time parameters, followed by the adaptive parameters, and finally the auxiliary system parameters.

Table 1. Control parameters (Part 1): BLF, fixed-time, adaptive RBFNN and auxiliary system.

Category	Symbol	Value
BLF parameters	$x_{\min}, x_{\max}$	$-315, 315$
	$y_{\min}, y_{\max}$	$t-3, t+3$
	ζ_1	0.4
	θ	3
	ε_1	0.1
	ε_2	0.05
Fixed-time convergence parameters	c_2	20
	c_3	1.2×10^6
	c_4	7×10^2
	c_5	2×10^4
	c_6	7×10^3
Adaptive and RBFNN parameters	$\lambda_1, \lambda_2, \lambda_3$	10, 4, 2
	$\lambda_4, \lambda_5, \lambda_6$	8, 3, 0.5
	η_1, η_2	$7 \times 10^5, 7 \times 10^3$
	η_3, η_4	$1.3 \times 10^5, 3.3 \times 10^7$
	σ_1, σ_2	$1.4 \times 10^{-15}, 1.4 \times 10^{-2}$
	σ_3, σ_4	$1.4 \times 10^{-4}, 1.4 \times 10^{-2}$
	σ_5, σ_6	$1.3 \times 10^{-17}, 13$
	σ_7, σ_8	$1 \times 10^{-22}, 1.3 \times 10^{-4}$
	b_1, b_2	18, 10
Vessel model parameters	m	1.18×10^5 kg
	m_{11}	1.2×10^5 kg
	m_{22}	1.779×10^5 kg
	m_{33}	6.36×10^7 kg
	d_{11}	2.15×10^4 kg/s
	d_{22}	1.47×10^5 kg/s
	d_{33}	8.02×10^6 kg/s

Table 1. *Cont.*

Category	Symbol	Value
Input and trajectory parameters	$\tau_{u,\max}, -\tau_{u,\min}$ $\tau_{r,\max}, -\tau_{r,\min}$ x_d y_d $(x_0, y_0, \psi_0, u_0, v_0, r_0)$	6.3×10^6 N 4×10^6 N·m $300\sin(0.03t)$ t $(20, 0, 0, 0, 1.0, 0)$
Auxiliary system parameters	T_r	0.1
Model uncertainty terms	Δf_u Δf_v Δf_r	$0.2d_{11}u^2 + 0.1d_{11}u^3$ $0.2d_{22}v^2 + 0.1d_{22}v^3$ $0.2d_{33}r^2 + 0.2d_{33}r^3$

Remark 1. *To evaluate the robustness of the proposed control framework with respect to parameter variations, four representative parameters associated with the BLF transformation, fixed-time controller, adaptive learning law, and auxiliary system are varied by ±20% around their nominal values. The corresponding results are summarized in Table 2. As shown in Table 2, moderate parameter variations mainly influence the transient convergence behavior, while the overall tracking accuracy remains largely unchanged. These results indicate that the proposed control framework possesses satisfactory robustness against parameter perturbations.*

Table 2. Robustness evaluation under representative parameter perturbations.

Parameter	Variation	RMSE-x	RMSE-y	RMSE-ψ	Settling Time
Baseline	Nominal	0.051	0.047	0.032	7.9
λ_1	−20% +20%	0.060 0.055	0.055 0.050	0.038 0.034	8.6 7.4
c_3	−20% +20%	0.068 0.054	0.062 0.049	0.041 0.033	9.3 7.0
η_1	−20% +20%	0.058 0.053	0.053 0.048	0.036 0.033	8.3 7.7
T_r	−20% +20%	0.064 0.056	0.058 0.051	0.039 0.035	8.8 7.5

Remark 2. *The robustness of the proposed BLF-based constraint mechanism is mainly challenged when the system operates close to the prescribed boundaries in the presence of uncertainties and external disturbances. In the adopted simulation, the reference trajectory amplitude reaches 300 m, while the admissible position boundary is limited to ±315 m, leaving only a 15 m safety margin. Consequently, the vessel repeatedly evolves in the vicinity of the constraint boundaries, where the BLF exhibits its strongest corrective action. Meanwhile, the controller must simultaneously compensate for initial tracking errors, unknown nonlinear dynamics, and environmental disturbances. The simulation results in Figures 2–6 show that all constrained states remain strictly within the predefined safe set and satisfactory tracking performance is maintained throughout the maneuvering process. These results indicate that the proposed BLF-based control framework preserves both constraint satisfaction and tracking accuracy under boundary-adjacent and uncertainty-affected operating conditions, thereby demonstrating its robustness under critical operating scenarios.*

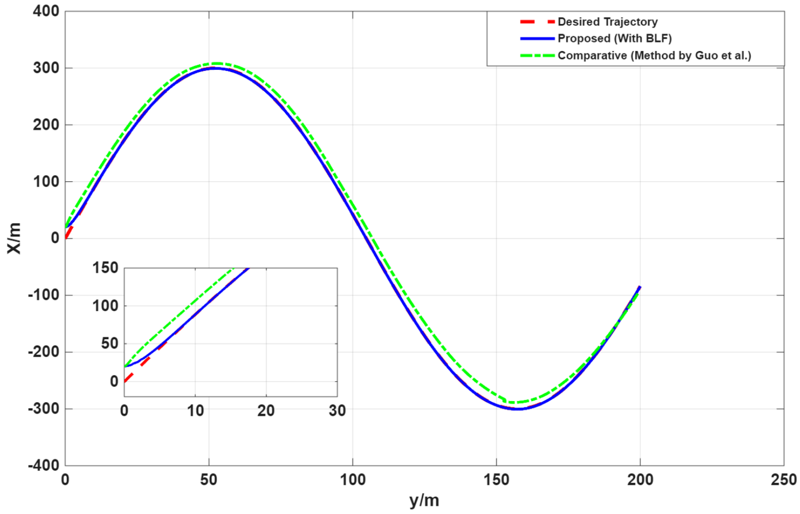

Figure 2. X-Y plane trajectory tracking comparison. The comparative scheme is proposed by Guo and Zhang X [50]: Adaptive path following control for autonomous surface vehicles towed by a single tugboat with output constraints.

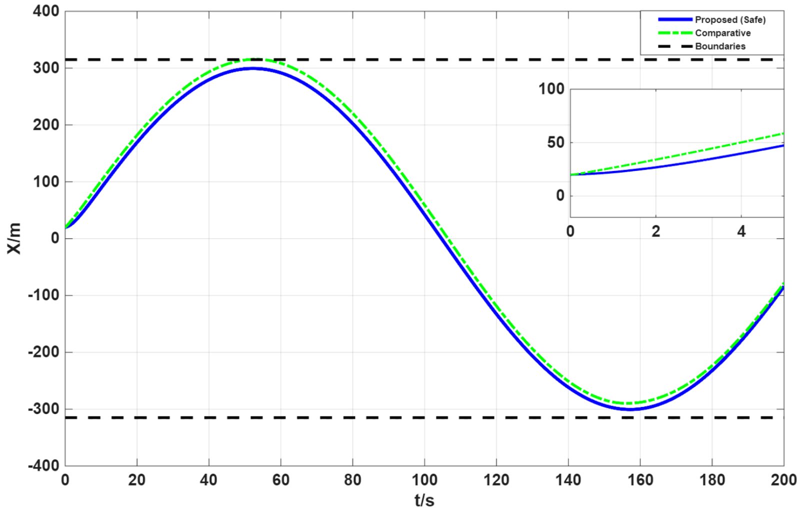

Figure 3. Longitudinal position and safety boundary comparison.

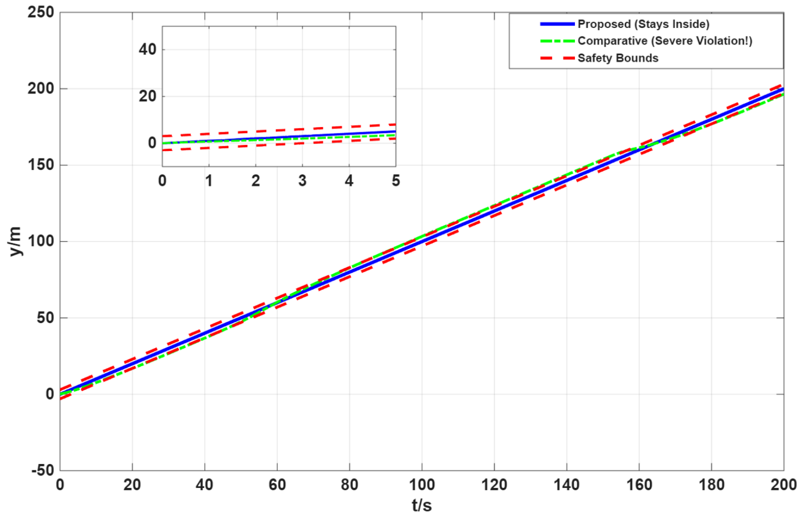

Figure 4. Lateral position and safety boundary comparison.

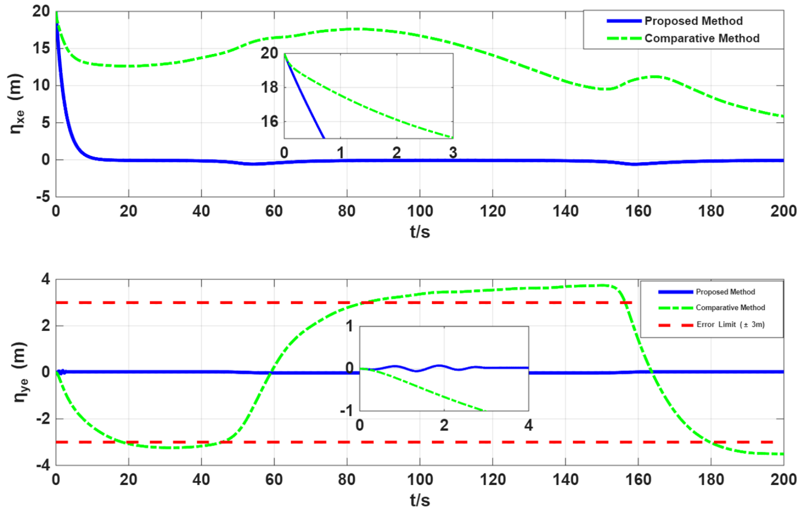

Figure 5. Position tracking error comparison.

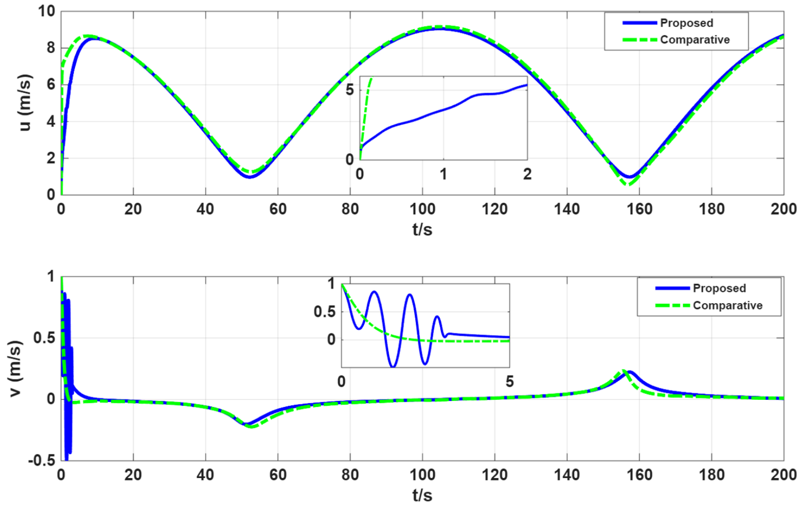

Figure 6. Velocity response comparison.

To comprehensively evaluate the superiority and practical necessity of the proposed control framework, a comparative simulation is conducted against the adaptive fixed-time path following control scheme proposed by Guo and Zhang (2025) [50], which employs a Barrier Lyapunov Function and RBF neural networks but lacks any compensation mechanism for actuator saturation. All simulations are carried out under identical initial conditions, time-varying ocean disturbances, model uncertainties, and actuator saturation limits.

Figure 2 presents the trajectory tracking performance in the X-Y plane. It can be observed that the proposed method accurately tracks the desired trajectory with smooth response and full compliance with the predefined position constraints. In contrast, the comparative method, which adopts an adaptive fixed-time path following control scheme based on the Barrier Lyapunov Function and RBF neural networks, exhibits notable tracking deviations and poor constraint satisfaction under the same conditions, leading to degraded practical performance. To quantitatively evaluate the tracking performance, the root mean square errors (RMSEs) of position and heading are summarized in Table 3. Compared with the adaptive fixed-time control scheme Guo & Zhang, 2025 [50], the proposed method achieves substantially smaller tracking errors, demonstrating superior accuracy. Furthermore, the total variation (TV) of the control inputs is computed to assess control smoothness, as shown in Table 4. The proposed method yields considerably lower TV values, indicating smoother control commands with significantly reduced chattering, which is beneficial for practical actuator operation. Figures 3 and 4 further illustrate the longitudinal and lateral position responses. The proposed method strictly confines the vessel position within the preset safety boundaries throughout the entire navigation process. In contrast, the adaptive fixed-time controller reported by Guo and Zhang (2025) [50] exhibits noticeable deviations from the prescribed safety region, particularly in the lateral direction, accompanied by larger position excursions. These results demonstrate that the incorporation of the symmetric BLF effectively guarantees state constraint satisfaction while improving navigation safety in restricted waterways. The position tracking errors are quantitatively compared in Figure 5. The proposed method drives both longitudinal and lateral tracking errors to converge rapidly to a very small neighborhood of zero within the predefined fixed time, with negligible steady-state errors and minimal oscillations. Meanwhile, the comparative controller presented by Guo and Zhang (2025) [50] produces relatively larger residual errors and slower convergence rates. The superior tracking accuracy of the proposed framework is further confirmed by the RMSE results reported in Table 3. As illustrated in Figure 6, the velocity responses of the proposed method are stable and rapid, demonstrating strong dynamic performance and satisfactory disturbance rejection capability. Compared with the controller of Guo and Zhang (2025) [50], the proposed strategy achieves faster velocity convergence and smaller transient fluctuations under the same disturbance conditions. Figure 7 presents the time histories of the control inputs. The control forces and moments generated by the proposed method remain strictly within the given actuator limits without noticeable chattering or saturation-induced clipping. By comparison, the controller of Guo and Zhang (2025) [50] exhibits larger transient control variations and less smooth control actions during the initial stage. The effectiveness of the fixed-time auxiliary system in handling input saturation is therefore validated. The oscillations in Figures 6 and 7 within 0–5 s result from the fixed-time convergence mechanism, the initial adaptation of zero-initialized RBF neural network, and the activation of the input-saturation auxiliary system (Equations (26) and (38)). According to the Lyapunov stability analysis in Section 4, all system signals remain bounded and the closed-loop system is stable. The oscillations decay quickly as adaptive parameters converge. Meanwhile, the vessel positions comply with BLF safety boundaries (Figures 3 and 4) and control inputs stay within actuator limits (Figure 7). Since the initial states deviate from the equilibrium, such transient fluctuations are inevitable. They represent a trade-off between fast fixed-time convergence and control smoothness, and will not affect the controller's stability and practical performance. Furthermore, Figure 8 validates that the RBF neural network approximates the unknown vessel dynamics effectively and smoothly. Figure 9 confirms that the designed adaptive laws estimate the upper bounds of compound disturbances with satisfactory stability. Finally, Figure 10 shows that the auxiliary system states converge rapidly within the fixed-time threshold, confirming that the auxiliary system compensates for saturation nonlinearities within the predefined time and avoids inducing high-frequency chattering.

Ultimately, these comprehensive results confirm that the integration of BLF, adaptive estimation, and fixed-time auxiliary systems is indispensable for safe, deterministic, and high-precision trajectory tracking of underactuated surface vessels in complex marine environments.

Table 3. Root mean square error of tracking results.

Control Scheme	RMSE-x (m)	RMSE-y (m)	RMSE-ψ (Rad)
Proposed Method	0.051	0.047	0.032
Adaptive fixed-time control (Guo & Zhang, 2025 [50])	0.273	0.254	0.186

Table 4. Total variation of control inputs.

Control Scheme	TV(τ_u) (N)	TV(τ_r) (N·m)
Proposed Method	63.1	71.5
Adaptive fixed-time control (Guo & Zhang, 2025 [50])	132.7	168.3

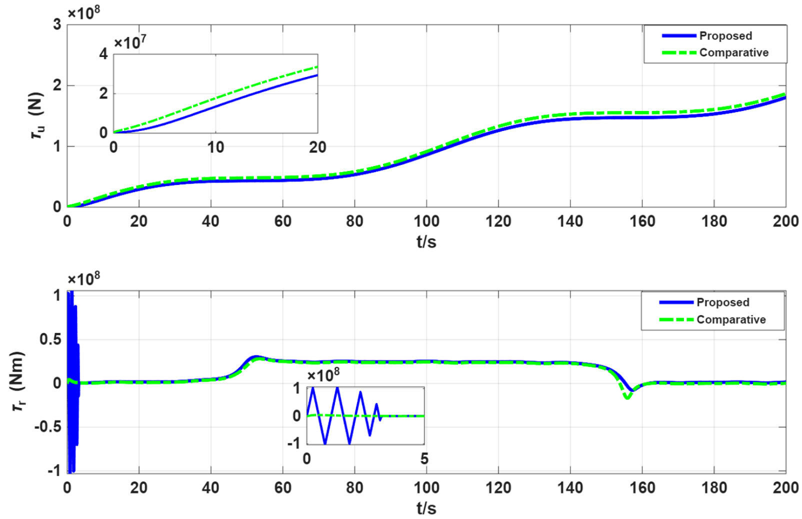

Figure 7. Control input comparison.

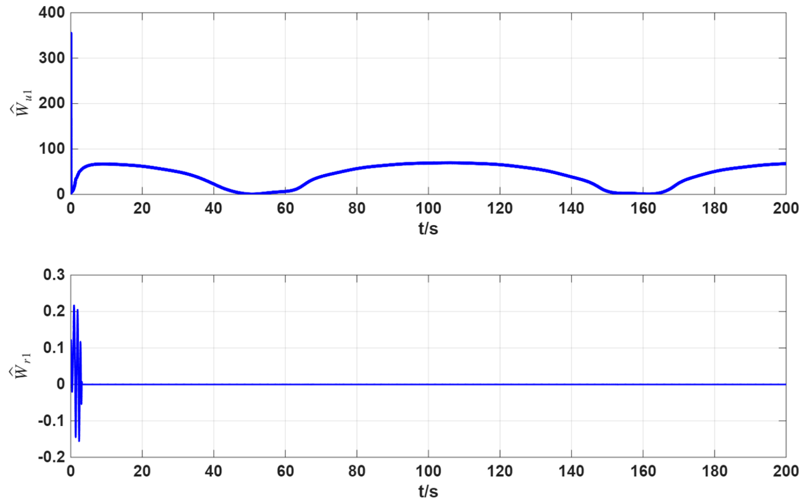

Figure 8. Neural network approximation performance.

Furthermore, to further evaluate the practical applicability of the proposed control framework, the computational cost of the controller is quantified and summarized in Table 5. The average computation time is 0.63 ms, while the maximum computation time is 1.12 ms. Both values are significantly lower than the adopted sampling interval of 10 ms. These results indicate that the proposed controller can complete all online computations within a single sampling period and therefore satisfies the requirements of real-time implementation. Although the control framework incorporates a symmetric BLF, adaptive RBF neural networks, and a fixed-time auxiliary system, the resulting computational burden remains moderate because the controller only involves algebraic calculations and adaptive update laws, without requiring iterative optimization procedures. Compared with optimization-based approaches such as model predictive control, the proposed method exhibits lower computational complexity and is therefore more suitable for real-time autonomous vessel applications deployed on embedded marine control platforms.

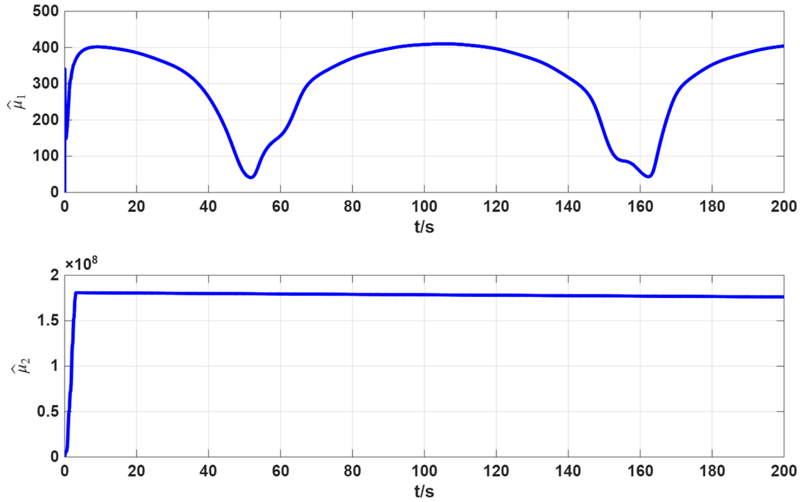

Figure 9. Adaptive estimation of compound disturbance upper bound.

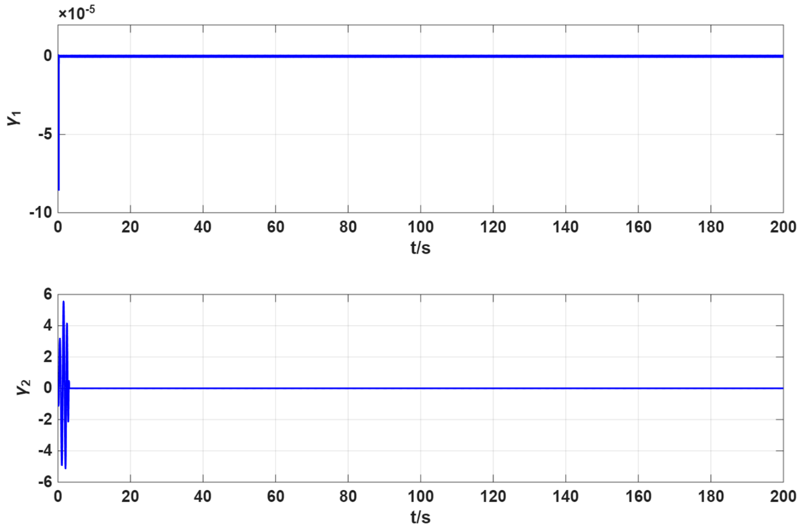

Figure 10. Convergence of fixed-time auxiliary system states.

Table 5. Computational cost evaluation.

Item	Value
Average computation time	0.63 ms
Maximum computation time	1.12 ms
Sampling period	10 ms

6. Conclusions

This paper presented the development of an adaptive fixed-time trajectory tracking controller for underactuated surface vessels with unknown dynamics, full state constraints, and input saturation. Compared with the existing results, the proposed scheme has some advantages: a deterministic convergence performance independent of initial states and strict constraint guarantee for both position and control input. The problems of constraint violation and actuator saturation are circumvented by a fusion of the BLF technique and fixed-time auxiliary system. The stability of the closed-loop system has been proven using the Lyapunov theory. Simulation results have been presented to demonstrate the effectiveness of the novel controller.

However, this work naturally cannot attend to every detail of the control design. We are working on an extension of our proposed scheme to address the following problems:

extension to more industrial systems—the proposed method can be further extended to practical systems such as permanent magnet synchronous motors and autonomous underwater vehicles, which have similar nonlinear and constrained characteristics; time-delay compensation—signal delay and input delay widely exist in practical engineering, which have important practical significance and deserve further in-depth investigation.

Author Contributions: Conceptualization, Q.G.; methodology, Q.G.; software, S.D. and J.Z.; validation, S.D. and J.Z.; formal analysis, Q.G.; investigation, Q.G.; resources, Q.G.; data curation, S.W. and R.L.; writing—original draft preparation, S.W. and R.L.; writing—review and editing, Q.G.; visualization, X.Z.; supervision, X.Z.; project administration, Q.G.; funding acquisition, Q.G. All authors have read and agreed to the published version of the manuscript.

Funding: This work was supported by the Xi'an Science and Technology Program (Grant No. 23ZDCYJSGG0025-2022), the Science Research Program of Shaanxi Educational Committee (Grant No. 23JC049), and the Natural Science Basic Research Program of Shaanxi (Grant No. 2021JQ-574).

Data Availability Statement: The original contributions presented in this study are included in the article. Further inquiries can be directed to the corresponding author.

Acknowledgments: Much appreciation to each reviewer for their insightful comments and suggestions, which have helped improve the quality of this paper.

Conflicts of Interest: The authors declare no conflicts of interest.

References

1. Zheng, Y.M.; Tao, J.; Hartikainen, J.; Duan, F.; Sun, H.; Sun, M.W.; Sun, Q.L.; Zeng, X.Y.; Chen, Z.Q.; Xie, G.M. Prescribed performance LOS guidance-based dynamic surface path following control of unmanned sailboats. *Ocean Eng.* **2023**, *271*, 113667.
2. Lei, Y.S.; Zhang, X.K.; Zhang, H.G.; Guo, Q. Prescribed performance ship trajectory tracking control with input and output constraints. *Ocean Eng.* **2025**, *341*, 122472. [CrossRef]
3. Yu, D.; Roh, M.I. Method for anti-collision path planning using velocity obstacle and A algorithms for maritime autonomous surface ship. *Int. J. Nav. Archit. Ocean Eng.* **2024**, *16*, 100586. [CrossRef]
4. Liu, C.; Hu, Q.; Wang, X.; Yin, J. Event-triggered-based nonlinear model predictive control for trajectory tracking of underactuated ship with multi-obstacle avoidance. *Ocean Eng.* **2022**, *253*, 111278. [CrossRef]
5. Shen, Z.; Liu, Y.; Nie, Y.; Yu, H. Prescribed performance LOS guidance-based dynamic surface path following control of unmanned sailboats. *Ocean Eng.* **2023**, *284*, 115182. [CrossRef]
6. Esmail, A.H.; Ghous, I.; Duan, Z.; Jaffery, M.H.; Li, S. Observer-based control for time-delayed quasi-one-sided Lipschitz nonlinear systems under input saturation. *J. Frankl. Inst.* **2024**, *361*, 107326. [CrossRef]
7. Liu, R.; Zhang, W.; Zhang, G.; Zhang, X. Disturbance observer-based adaptive neural control for underactuated surface vehicle with constraint of input saturation. *Ocean Eng.* **2023**, *287*, 115744. [CrossRef]
8. Li, L.; Wang, C.; Lu, K.; Wu, Z.; Deng, F. FTUVE based global fast terminal backstepping sliding mode control for dynamic positioning ships. *Ocean Eng.* **2025**, *336*, 121709. [CrossRef]
9. Zhang, Y.; Zhang, J.; Sui, B. Robust fixed-time adaptive fault-tolerant control for dynamic positioning of ships with thruster faults. *Appl. Sci.* **2024**, *14*, 5738. [CrossRef]
10. Wang, Z.; Wu, Y.; Chu, X.; Liu, C.; Zheng, M. Risk identification method for ship navigation in the complex waterways via consideration of ship domain. *J. Mar. Sci. Eng.* **2023**, *11*, 2265. [CrossRef]
11. Liu, X.; He, Y.; Zhang, K.; Mou, J.; Zhang, K.; Zhao, X. Research on the decision-making method for autonomous navigation for the ocean-going ship in the ships' routeing waters. *Ocean Eng.* **2025**, *223*, 120641. [CrossRef]
12. Shu, Y.; Xiong, C.; Zhu, Y.; Liu, K.; Liu, R.W.; Xu, F.; Zhang, L. Reference path for ships in ports and waterways based on optimal control. *Ocean Coast. Manag.* **2024**, *253*, 107168. [CrossRef]
13. Li, H.; Lin, X. Robust fault-tolerant control for dynamic positioning of ships with prescribed performance. *Ocean Eng.* **2024**, *298*, 117314. [CrossRef]
14. Liu, Z.; Zhao, Y.; Zhang, O.; Gao, Y.; Liu, J. Adaptive fuzzy neural network-based finite time prescribed performance control for uncertain robotic systems with actuator saturation. *Nonlinear Dyn.* **2024**, *112*, 12171–12190. [CrossRef]
15. Li, J.; Xiang, X.; Zhang, Q.; Yang, S. Robust practical prescribed time trajectory tracking of USV with guaranteed performance. *Ocean Eng.* **2024**, *302*, 117622. [CrossRef]

16. Wang, Y.; Wang, H.; Li, M.; Wang, D.; Fu, M. Adaptive fuzzy controller design for dynamic positioning ship integrating prescribed performance. *Ocean Eng.* **2021**, *219*, 107956. [CrossRef]
17. Dong, C.; Zheng, B.; Chen, L. Trajectory tracking control for uncertain underactuated surface vessels with guaranteed prescribed performance under stochastic disturbances. *Nonlinear Dyn.* **2024**, *112*, 13215–13231. [CrossRef]
18. Qin, J.; Du, J. Practically prescribed-time trajectory tracking control for underactuated SVs with input and output constraints under parametric uncertainties. *Ocean Eng.* **2025**, *341*, 122344. [CrossRef]
19. Zhou, B.; Hu, C.; Jin, G.; Yu, J.; Jiang, X.; Zhang, G. Design of UDE-based finite-time fault-tolerant control for DP vessels with complex disturbances and input constraints. *Ocean Eng.* **2023**, *287*, 115774. [CrossRef]
20. Yin, Z.; Wang, W.; Liu, Z.; Liu, F. Fixed-time control of a marine surface vessel system with input saturation and guaranteed prescribed constraints. *Ocean Eng.* **2024**, *297*, 117078. [CrossRef]
21. Sui, B.; Zhang, J.; Liu, Z.; Wei, J. Fixed-Time Trajectory Tracking Control of Fully Actuated Unmanned Surface Vessels with Error Constraints. *J. Mar. Sci. Eng.* **2024**, *12*, 584. [CrossRef]
22. Wu, J.; Li, B.; Li, J.; Li, M.; Yang, B. Global Stabilization of Control Systems with Input Saturation and Multiple Input Delays. *Actuators* **2024**, *13*, 306. [CrossRef]
23. Zhang, B.; Liang, Y.; Rao, S.; Kuang, Y.; Zhu, W. RBFNN-based anti-input saturation control for hypersonic vehicles. *Aerospace* **2024**, *11*, 108. [CrossRef]
24. Sui, B.; Zhang, J.; Liu, Z.; Wei, J. Distributed prescribed-time cooperative formation tracking control of networked unmanned surface vessels under directed graph. *Ocean Eng.* **2024**, *305*, 117993. [CrossRef]
25. Wang, Z.; Qiu, C.; Dong, Z.; Cheng, S.; Zheng, L.; Chen, S. Trajectory tracking of unmanned surface vessels based on robust neural networks and adaptive control. *J. Mar. Sci. Eng.* **2025**, *13*, 1341. [CrossRef]
26. Wei, J.; Zhang, J.; Dong, H.; Liu, Z. Prescribed-time trajectory tracking control for underactuated USV with input amplitude and rate constraints. *Ocean Eng.* **2025**, *326*, 120891. [CrossRef]
27. Li, J.; Xiang, X.; Dong, D.; Yang, S. Prescribed time observer based trajectory tracking control of autonomous underwater vehicle with tracking error constraints. *Ocean Eng.* **2023**, *274*, 114018. [CrossRef]
28. Chen, J.; Yuan, J.; Li, R. Error-Constrained Fixed-Time Synchronized Trajectory Tracking Control for Unmanned Airships with Disturbances. *Drones* **2025**, *9*, 403. [CrossRef]
29. Guo, S.; Wang, L.; Fu, J. Adaptive Attitude Roll Control of Guided Projectile Based on a Novel Unidirectional Global Sliding Mode Algorithm. *Aerospace* **2024**, *11*, 683. [CrossRef]
30. Huang, H.; Gao, J. Backstepping and novel sliding mode trajectory tracking controller for wheeled mobile robots. *Mathematics* **2024**, *12*, 1458. [CrossRef]
31. Jiao, S.; Wang, J.; Hua, Y.; Zhuang, Y.; Yu, X. Trajectory-tracking control for quadrotors using an adaptive integral terminal sliding mode under external disturbances. *Drones* **2024**, *8*, 67. [CrossRef]
32. Wu, J.; Liu, H.; Li, B.; Li, J.; Li, M. Precision trajectory control in underwater vehicle-manipulator systems using advanced sliding mode techniques and state estimation. *Ocean Eng.* **2025**, *318*, 120129. [CrossRef]
33. Wang, J.; Li, Y.; Wu, Y.; Liu, Z.; Chen, K.; Chen, C.P. Fixed-time formation control for uncertain nonlinear multiagent systems with time-varying actuator failures. *IEEE Trans. Fuzzy Syst.* **2024**, *32*, 1965–1977. [CrossRef]
34. Ding, F.; Liu, X. High-order fast fixed-time sliding mode single-loop control for PMSM with disturbance compensator. *Control Eng. Pract.* **2025**, *164*, 106509. [CrossRef]
35. Yang, Y.; Tang, L.; Zou, W.; Ding, D.W.; Ahn, C.K. A unified fixed-time framework of adaptive fuzzy controller design for unmodeled dynamical systems with intermittent feedback. *Inf. Sci.* **2022**, *611*, 628–648. [CrossRef]
36. Khodaverdian, M.; Hajshirmohamadi, S.; Hakobyan, A.; Ijaz, S. Predictor-based constrained fixed-time sliding mode control of multi-UAV formation flight. *Aerosp. Sci. Technol.* **2024**, *148*, 109113. [CrossRef]
37. Guan, T.; Zhang, K.; Li, B.; Guan, X.; Yiu, K.F.C. Adaptive fixed-time sliding mode control for spacecraft reorientation with attitude pointing constraints and disturbance rejection. *ISA Trans.* **2023**, *143*, 50–58. [CrossRef] [PubMed]
38. Tang, L.; Liu, J.; Wang, L.; Wang, Y. Robust fixed-time trajectory tracking control of the dynamic positioning ship with actuator saturation. *Ocean Eng.* **2023**, *284*, 115199. [CrossRef]
39. Li, Y.; Bao, C.; Guo, R. Adaptive Fuzzy Sliding-Mode Control for Ship Path Tracking Based on a Fixed-Time Disturbance Observer. *J. Mar. Sci. Eng.* **2025**, *13*, 1788. [CrossRef]
40. Huang, X.; Liu, H.; Tian, X. Predefined time tracking control of underactuated surface vessel with input saturation. *Chin. J. Ship Res.* **2024**, *19*, 98–110.
41. Liu, Z.; Gong, Q.; Hu, X.; Zhu, G.; Guo, S.; Ma, B.; Li, X. Practical fixed-time formation control with disturbance rejection for marine vehicles under input saturation. *ISA Trans.* **2025**, *159*, 112–122.
42. Sui, B.; Liu, Y.; Zhang, J.; Liu, Z.; Zhang, Y. Prescribed-Time Trajectory Tracking Control for Unmanned Surface Vessels with Prescribed Performance Considering Marine Environmental Interferences and Unmodeled Dynamics. *J. Mar. Sci. Eng.* **2024**, *12*, 1380. [CrossRef]

43. Li, Z.; Lei, K. Robust fixed-time fault-tolerant control for USV with prescribed tracking performance. *J. Mar. Sci. Eng.* **2024**, *12*, 799. [CrossRef]
44. Deng, Y.; Zhang, X.; Zhao, D.; Ni, T.; Gong, M.; Zhang, Z. Adaptive neural network asymptotic path-following control of underactuated ships with stochastic sea loads. *Ocean Eng.* **2022**, *266*, 113147. [CrossRef]
45. Liu, Y.; Zhao, L.; Sun, W.; Wang, Q.; Li, G.; Guo, H.; Bai, Z. Event-triggered finite-time tracking control of unmanned surface vessel using neural network prescribed performance. *IEEE Access* **2023**, *12*, 11481–11491. [CrossRef]
46. Liu, Z. Ship adaptive course keeping control with nonlinear disturbance observer. *IEEE Access* **2017**, *5*, 17567–17575. [CrossRef]
47. Zhang, W.; Li, Y.; Wang, N. Adaptive sliding mode control design for nonlinear unmanned surface vessel using RBFNN and disturbance-observer. *IEEE Access* **2021**, *9*, 121458–121468.
48. Zhang, Q.; Guo, C. Anti-disturbance lyapunov-based model predictive control for trajectory tracking of dynamically positioned ships. *J. Mar. Sci. Eng.* **2023**, *11*, 281. [CrossRef]
49. Zhang, Z.; Wu, Y. Further results on fixed-time stabilization and tracking control of a marine surface ship subjected to output constraints. *IEEE Trans. Syst. Man Cybern. Syst.* **2019**, *51*, 5300–5310. [CrossRef]
50. Guo, Q.; Zhang, X. Adaptive path following control for autonomous surface vehicles towed by a single tugboat with output constraints. *ISA Trans.* **2025**, *162*, 75–84. [CrossRef] [PubMed]